ISBN: 978-3-95450-261-5 ISSN: 2673-7000 doi: 10.18429/JACoW-NAPAC2025-WEP015

# CO-SPUTTER DEPOSITION OF $Nb_3Sn$ LAYER INTO SRF CAVITY USING Nb-Sn COMPOSITE TARGET*

M. S. Shakel[1,†], H. E. Elsayed-Ali[1], G. Eremeev[2], U. Pudasaini[3], A. Valente-Feliciano[3]
[1]Old Dominion University, Norfolk, VA, USA
[2]Fermi National Accelerator Laboratory, Batavia, IL, USA
[3]Thomas Jefferson National Accelerator Facility, Newport News, VA, USA

*Abstract*

$Nb_3Sn$, with its superior superconducting critical temperature ($T_c$ ~18.3 K) and superheating magnetic field ($H_{sh}$ ~400 mT), is considered a promising material for superconducting radiofrequency (SRF) cavities, offering enhanced cryogenic performance compared to bulk Nb cavities. A $Nb_3Sn$ coating technique has been developed for SRF cavities using co-sputtering of Nb-Sn composite target in a DC cylindrical magnetron sputtering system. The composite target configuration and discharge conditions for co-sputtering were optimized to deposit Nb-Sn films on flat Nb substrates, followed by annealing to form $Nb_3Sn$. Several methods have been explored to improve the surface homogeneity of the $Nb_3Sn$ coating, including optimizing a two-step annealing process and a light Sn recoating process. A 1.5 µm Nb-Sn co-sputtered film was deposited on the interior of a 2.6 GHz Nb SRF cavity and annealed at 600 $^0$C for 6 h, followed by 950 $^0$C for 1 h. Cryogenic RF testing of the annealed cavity demonstrated a $T_c$ of 17.8 K, confirming the formation of $Nb_3Sn$. Then, the annealed cavity underwent a light Sn recoating treatment and attained a quality factor ($Q_0$) of 8.5E+08 at 2.0 K.

## INTRODUCTION

SRF cavities made from high-purity Nb have played a central role in modern particle accelerators due to their excellent superconducting properties and ease of fabrication into complex structures [1-5]. Significant progress in cavity performance has been achieved through advancing surface preparation techniques such as electropolishing, doping, and heat treatments to improve the Nb cavity surface quality [6-9]. However, bulk Nb cavities are now approaching their fundamental performance limits in terms of accelerating gradient and surface resistance [10, 11]. $Nb_3Sn$, an A15 compound, offers several advantages over Nb, including a higher $T_c$ and $H_{sh}$, nearly double those of Nb, can improve SRF cavity efficiency and enable operation at elevated temperatures, thereby reducing cryogenic load and operating costs [12-14]. The most widely used method for coating $Nb_3Sn$ onto Nb cavities is Sn vapor diffusion [15-17]. Recently, a cryomodule based on vapor diffused $Nb_3Sn$ coated Nb cavities has demonstrated an accelerating gradient of about 10 MV/m with low cryogenic loss at 4.4 K [18]. While effective, this process presents challenges such as the need for stringent control on Sn evaporation sources, non-uniform patchy regions, Sn-deficient areas on the coating layer, and the requirement for high processing temperatures [16, 19]. Magnetron sputtering is an alternative method offering improved control over film stoichiometry, deposition rate, and lower substrate temperatures [20-22]. We discuss the deposition of $Nb_3Sn$ onto a 2.6 GHz Nb SRF cavity using a composite Nb-Sn target inside a custom-designed DC cylindrical magnetron sputtering system [23]. The process development includes optimization of the co-sputtering target configuration and plasma discharge conditions to achieve suitable stoichiometry, followed by optimizing post-deposition annealing methods, including using a light Sn recoating. Lastly, cryogenic RF test results of the co-sputtered $Nb_3Sn$ coated cavity are presented.

## CO-SPUTTERING DEPOSITION OF NB-SN ON FLAT SUBSTRATES

To identify the optimum composite Nb-Sn target configuration and discharge condition, several combinations of Nb and Sn ring targets (OD 0.9", ID 0.8") were tested using the bottom magnetron of the cylindrical sputter coater. The lengths of the Nb and Sn targets in the composite configuration were adjusted to achieve the desired Nb-Sn stoichiometry in the sputtered film. The target configuration shown in Fig. 1(a) was identified as optimal. Fig. 1(b) shows the corresponding plasma discharge at 11 mTorr Ar pressure for 53 mA discharge current. One strong plasma glow ring appears around the central Nb target, while three weaker glow rings are observed around the Sn targets. These glow rings correspond to the magnetic field distribution across the magnetron surface [23]. Using this target configuration, Nb-Sn films were deposited on flat Nb substrates ($10 \times 10 \times 3$ mm$^3$) mounted at three representative locations of a mock 2.6 GHz SRF cavity: at top beam tube, equator, and bottom beam tube. Before deposition, the chamber's base pressure reached $2 \times 10^{-7}$ Torr. The magnetron speed was adjusted to ensure uniform coating thickness, and ~0.5 µm thick Nb-Sn films were deposited on Nb samples at the beam tubes and equator.

* This work is supported by DOE, Office of Accelerator R&D and Production, Contract No. DE-SC0022284. With partial support by DOE, Office of Nuclear Physics DE-AC05-06OR23177 to JLab and Contract No. DE-AC02-07CH11359, and Early Career Award to G. Eremeev. This manuscript has been authored by FermiForward Discovery Group, LLC under Contract No. 89243024CSC000002 with the DOE, Office of Science, Office of High Energy Physics.
† Email: mshak001@odu.edu

ISBN: 978-3-95450-261-5 ISSN: 2673-7000 doi: 10.18429/JACoW-NAPAC2025-WEP015



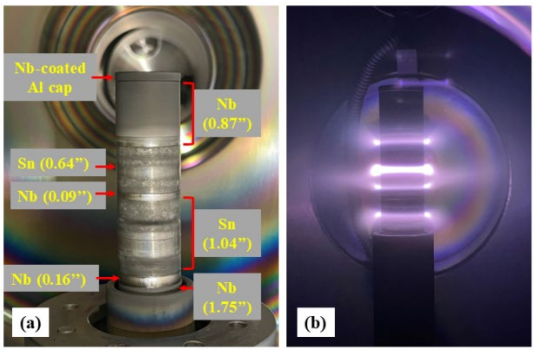


Figure 1: (a) Composite Nb-Sn target configuration used for co-sputter deposition, (b) Plasma discharge during co-sputtering at 11 mTorr Ar pressure using the composite Nb-Sn target.

## ANNEALING FOR IMPROVED SURFACE HOMOGENEITY

The sputtered films on Nb substrates were annealed in a high-vacuum furnace at Jefferson Lab to facilitate $Nb_3Sn$ phase formation by reacting Nb and Sn in the as-deposited Nb-Sn layer [17]. The annealing process began once the base pressure of the Nb insert accommodating the samples inside the furnace chamber was pumped down to the low $10^{-5}$ Torr or better. The furnace temperature ramped at 12 °C/min from room temperature to 950 ± 10 °C, followed by a 3 h hold at that temperature.

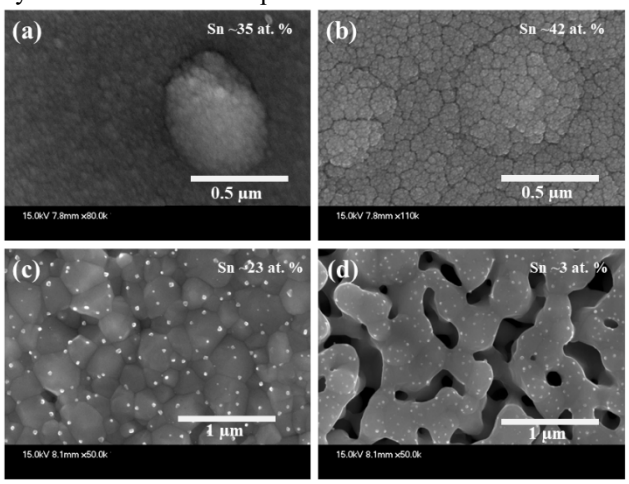


Figure 2: Surface morphology of co-sputtered films using the composite Nb-Sn target: as-deposited (a) top beam tube and (b) equator sample; 950 °C - 3 h annealed (c) top beam tube and (d) equator sample.

Energy-dispersive X-ray spectroscopy (EDS) analysis showed that the as-deposited samples contained ~32-42 at. % of Sn. Scanning electron microscopy (SEM) images revealed that the as-deposited samples did not exhibit well-formed grains, rather showed randomly oriented, nanoscale particle-like features, as shown in Fig. 2(a) and Fig. 2(b). After annealing at 950 °C for 3 h, X-ray diffraction (XRD) patterns confirmed the formation of $Nb_3Sn$ in all annealed samples, each exhibiting a polycrystalline $Nb_3Sn$ phase, without any diffraction peak corresponding to other Nb-Sn phases. EDS measurements of the annealed top beam tube and bottom beam tube samples indicated ~23 at. % Sn content. However, the annealed equator sample showed a significantly lower Sn content of ~3 at. %. SEM analysis demonstrated that the surfaces of the annealed beam tube samples consisted of homogeneous and uniformly distributed $Nb_3Sn$ grains with clearly defined boundaries and an average grain size of ~260 nm, as shown in Fig. 2(c). However, the annealed equator sample exhibited elongated $Nb_3Sn$ structures with poorly defined grain boundaries and large porous regions across the surface, as shown in Fig. 2(d).

This disparity is likely due to the equator sample being located at ~40 mm from the sputter target surface, compared to the beam tube surfaces, which were only ~8 mm away, allowing more magnetron plasma interaction during deposition. Also, the surface voids observed in the as-deposited equator sample (Fig. 2 (b)) may have provided pathways for rapid Sn evaporation during annealing, leading to significant Sn loss. Small particle-like structures ranging from 17 to 36 nm in size were observed on the surfaces of annealed samples.

SEM images of top beam tube samples annealed at 600 °C for 1 h, followed by 950 °C for 3 h and annealed at 600 °C for 6 h, followed by 950 °C for 1 h are shown in Fig. 3(a) and 3(b), respectively. In both annealing conditions, the top beam tube sample demonstrated well-formed $Nb_3Sn$ grains without any voids.

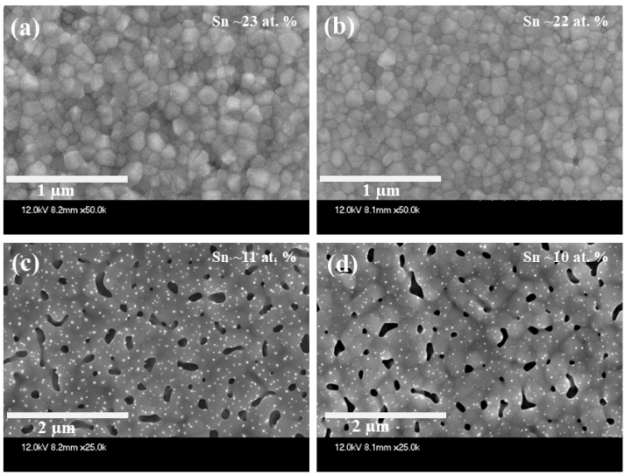


Figure 3: SEM images of top beam tube samples annealed at (a) 600 °C for 1 h, followed by 950 °C for 3 h and (b) 600 °C for 6 h, followed by 950 °C for 1 h. Corresponding SEM images of annealed equator samples are shown in (c) and (d), which underwent similar annealing steps as (a) and (b), respectively.

Several approaches were investigated to mitigate Sn evaporation and reduce void density in the equator sample during post-sputter annealing. An additional lower temperature annealing step at 600 °C was introduced prior to the 950 °C annealing, and the optimum duration for this step was determined. Additionally, the annealing duration at 950 °C was reduced from 3 h to 1 h to minimize Sn loss. It was observed that the equator sample, which underwent annealing at 600 °C for 1 h, followed by 950 °C for 3 h,

ISBN: 978-3-95450-261-5 ISSN: 2673-7000 doi: 10.18429/JACoW-NAPAC2025-WEP015

demonstrated a surface void coverage area of about 16%, as shown in Fig. 3(c), a significant reduction compared to 25 % void coverage observed without 600 °C preliminary annealing, as seen in Fig 2(d). Another equator sample, which underwent annealing at 600 °C for 6 h, followed by 950 °C for 1 h, exhibited a surface void coverage area of about 9 %, as shown in Fig. 3(d). The Sn content in both annealed equator samples increased to 10–11 at.%.

We explored an additional surface treatment involving light recoating using Sn vapor diffusion at Fermilab, which has previously been applied on $Nb_3Sn$ coated 1.3 GHz Nb cavities to heal cracks in the $Nb_3Sn$ layer [24]. In our study, light Sn recoating was applied to eliminate voids and enhance surface homogeneity in the annealed co-sputtered samples. The top beam tube and equator samples, annealed at 600 °C for 6 h followed by 950 °C for 1 h, underwent the light Sn recoating process. The treatment successfully eliminated surface voids and improved surface homogeneity by promoting the formation of well-defined grains through Sn diffusion into void regions, enabling $Nb_3Sn$ growth at those locations. Upon the recoating process, the equator sample exhibited larger $Nb_3Sn$ grains, with grain sizes reaching up to 975 nm in diameter, as shown in Fig. 4(b), compared to the top beam tube sample, as shown in Fig. 4(a).

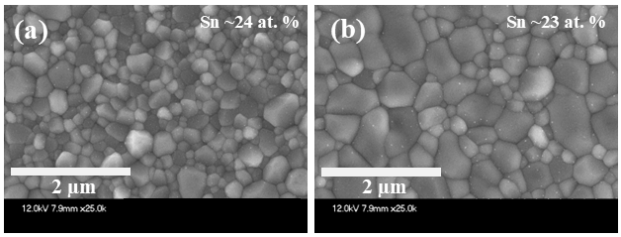


Figure 4: SEM images of (a) top beam tube and (b) equator samples after light Sn recoating treatment. Prior to recoating, both co-sputtered Nb-Sn films were annealed at 600 °C for 6 h, followed by 950 °C for 1 h.

## CO-SPUTTERING DEPOSITION ON NB CAVITY

An anodized single-cell 2.6 GHz Nb SRF cavity, fabricated from high-purity Nb, was installed in the deposition chamber for Nb-Sn coating using the composite target configuration shown in Fig. 1(a). The magnetron discharge was carried out at 47 mA after the base pressure reached $1.9 \times 10^{-7}$ Torr. During deposition, the discharge power was varied between 16.7 and 17.6 W. At the same time, the magnetron moved inside the SRF cavity, resulting in the deposition of about 1.5 µm of co-sputtered Nb-Sn film. The coated cavity underwent high-pressure rinsing at 50 bar using ultra-pure deionized water. The as-deposited surface appeared visually uniform, with a consistent appearance across the cavity and no visible signs of film peeling or surface residues. Next, the cavity was placed inside a Nb box and transferred to a high-vacuum furnace at Fermilab for annealing. Once the furnace reached a base pressure of about $8.8 \times 10^{-7}$ Torr after installing the cavity inside, a degassing step was performed at 200 °C for 60 h. The annealing procedure began with a temperature ramp of 3 °C/min to 600 °C, where it was held for 6 h. This was followed by a ramp of 12 °C/min to 950 °C, with a 1 h hold at that temperature. After annealing, the cavity surface displayed a uniform, slightly whitish coloration across its entire surface. The annealed cavity was removed from the furnace and prepared in a cleanroom for cryogenic RF testing in the vertical test stand system at Fermilab. The temperature dependence of the loaded quality factor ($Q_L$) exhibited two distinct transitions: one at about 17.8 K, corresponding to the $T_c$ of the $Nb_3Sn$ layer, and another at about 7.4 K, attributed to possible Sn-deficient $Nb_3Sn$ in the equator region of the cavity. The cavity then underwent a light recoating treatment using Sn vapor diffusion, following the procedure described in [24].

The $Q_0$ versus $E_{acc}$ performance of the light recoated 2.6 GHz Nb cavity was measured at cryogenic temperatures. As shown in Fig. 5, the cavity achieved a quality factor $Q_0$ of $1.5 \times 10^8$ at low fields at 4.2 K, with the accelerating gradient $E_{acc}$ limited to 4 MV/m. The low field $Q_0$ increased to $8.5 \times 10^8$ at 2.0 K, with $E_{acc}$ constrained to 6.1 MV/m. The $T_c$ of the Sn-recoated cavity was measured to be about 17.6 K, attributed to the $Nb_3Sn$ layer.

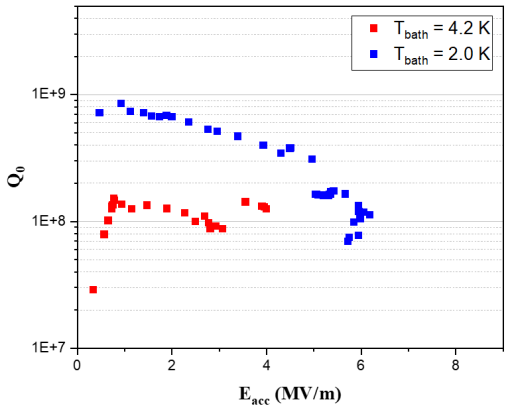


Figure 5: $Q_0$ versus $E_{acc}$ performance after recoating of the 2.6 GHz Nb cavity. Prior to light vapor diffusion coating, approximately 1.5 µm of $Nb_3Sn$ was deposited inside the cavity via co-sputtering, followed by annealing at 600 °C for 6 h and then 950 °C for 1 h.

## CONCLUSION

$Nb_3Sn$ coating was deposited by co-sputtered Nb-Sn films on flat Nb substrates. Annealing processes were explored to reduce surface voids and improve Sn retention in the annealed films. A ~1.5 µm thick co-sputtered Nb-Sn layer was deposited inside a 2.6 GHz Nb SRF cavity. The cavity was annealed at 600 °C for 6 h, followed by 950 °C for 1 h. During cryogenic RF testing, the annealed cavity exhibited a $T_c$ of about 17.8 K. After undergoing a light Sn vapor diffusion coating, the cavity demonstrated a $Q_0$ of $8.5 \times 10^8$ at low fields, with $E_{acc}$ limited to 6.1 MV/m at 2.0 K.

ISBN: 978-3-95450-261-5 ISSN: 2673-7000 doi: 10.18429/JACoW-NAPAC2025-WEP015



# REFERENCES


[1] P. A. Adderley *et al.*, "The Continuous Electron Beam Accelerator Facility at 12 GeV," *Phys. Rev. Accel. Beams*, vol. 27, no. 8, p. 084802, Aug. 2024. doi:10.1103/physrevaccelbeams.27.084802

[2] V. S. Morozov, C. C. Peters, and A. P. Shishlo, "Oak Ridge Spallation Neutron Source superconducting rf linac availability performance and demonstration of operation restoration with superconducting rf cavity off," *Phys. Rev. Accel. Beams*, vol. 25, no. 2, p. 020101, Feb. 2022. doi:10.1103/physrevaccelbeams.25.020101

[3] W. Singer *et al.*, "Superconducting cavity material for the European XFEL," *Supercond. Sci. Technol.*, vol. 28, no. 8, p. 085014, Jul. 2015. doi:10.1088/0953-2048/28/8/085014

[4] M. C. Ross, "LCLS-II: status, issues and plans", in *Proc. SRF'19*, Dresden, Germany, Jun.-Jul. 2019, pp. 1-8. doi:10.18429/JACoW-SRF2019-MOFAA1

[5] A. M. Rowe *et al.*, "Cavity processing and preparation of 650 MHz elliptical cell cavities for PIP-II", in *Proc. LINAC'16*, East Lansing, MI, USA, Sep. 2016, pp. 229-232. doi:10.18429/JACoW-LINAC2016-MOPLR043

[6] V. Chouhan *et al.*, "Electropolishing parameters study for surface smoothening of low-β 650 MHz five-cell niobium superconducting radio frequency cavity," *Nucl. Instrum. Methods Phys. Res. A*, vol. 1051, p. 168234, Jun. 2023. doi:10.1016/j.nima.2023.168234

[7] P. Dhakal, "Nitrogen doping and infusion in SRF cavities: A review," *Phys. Open*, vol. 5, p. 100034, Dec. 2020. doi:10.1016/j.physo.2020.100034

[8] B. Abdisatarov *et al.*, "Optimizing superconducting Nb film cavities by mitigating medium-field Q-slope through annealing," *Supercond. Sci. Technol.*, vol. 38, no. 7, p. 075006, Jun. 2025. doi:10.1088/1361-6668/ade635

[9] J. K. Tiskumara, J. R. Delayen, G. V. Eremeev, and U. Pudasaini, "Lower temperature annealing of vapor diffused $Nb_3Sn$ for accelerator cavities", in *Proc. NAPAC'22*, Albuquerque, NM, USA, Aug. 2022, pp. 695-698. doi:10.18429/JACoW-NAPAC2022-WEPA31

[10] H. Padamsee, "50 years of success for SRF accelerators—a review," *Supercond. Sci. Technol.*, vol. 30, no. 5, p. 053003, Apr. 2017. doi:10.1088/1361-6668/aa6376

[11] S. Posen and M. Liepe, "SRF cavities beyond niobium: challenges and potential", in *Proc. NAPAC'13*, Pasadena, CA, USA, Sep.-Oct. 2013, paper WEZBA1, pp. 754-758.

[12] S. Posen, M. Liepe, G. Eremeev, U. Pudasaini, C.E. Reece, "$Nb_3Sn$ superconducting radiofrequency cavities: a maturing technology for particle accelerators and detectors," *White Paper for Snowmass 2021*, https://lss.fnal.gov/archive/2022/conf/fermilab-conf-22-321-td.pdf

[13] S. Posen and D. L. Hall, "$Nb_3Sn$ superconducting radiofrequency cavities: fabrication, results, properties, and prospects," *Supercond. Sci. Technol.*, vol. 30, no. 3, p. 033004, Jan. 2017. doi:10.1088/1361-6668/30/3/033004

[14] S. Posen, M. Liepe, and D. L. Hall, "Proof-of-principle demonstration of $Nb_3Sn$ superconducting radiofrequency cavities for high Q applications," *Appl. Phys. Lett.*, vol. 106, no. 8, Feb. 2015. doi:10.1063/1.4913247

[15] U. Pudasaini, G. V. Eremeev, J. W. Angle, J. Tuggle, C. E. Reece, and M. J. Kelley, "Growth of $Nb_3Sn$ coating in tin vapor-diffusion process," *J. Vac. Sci. Technol., A*, vol. 37, no. 5, Aug. 2019. doi:10.1116/1.5113597

[16] J. Lee *et al.*, "Atomic-scale analyses of $Nb_3Sn$ on Nb prepared by vapor diffusion for superconducting radiofrequency cavity applications: a correlative study," *Supercond. Sci. Technol.*, vol. 32, no. 2, p. 024001, Dec. 2018. doi:10.1088/1361-6668/aaf268

[17] G. Eremeev *et al.*, "$Nb_3Sn$ multicell cavity coating system at Jefferson Lab," *Rev. Sci. Instrum.*, vol. 91, no. 7, p. 073911, Jul. 2020. doi:10.1063/1.5144490

[18] G. Eremeev *et al.*, "Demonstration of $E_{acc} = 10$ MV m$^{-1}$ with $Nb_3Sn$ cavities in a cryomodule," *Supercond. Sci. Technol.*, vol. 38, no. 7, p. 07LT01, Jul. 2025. doi:10.1088/1361-6668/ade82d

[19] U. Pudasaini, M. J. Kelley, G. V. Eremeev, C. E. Reece, and J. Tuggle, "Insights into formation of $Nb_3Sn$ film during the vapor diffusion process", in *Proc. SRF'17*, Lanzhou, China, Jul. 2017, pp. 539-542. doi:10.18429/JACoW-SRF2017-TUPB067

[20] M. N. Sayeed, U. Pudasaini, C. E. Reece, G. Eremeev, and H. E. Elsayed-Ali, "Structural and superconducting properties of $Nb_3Sn$ films grown by multilayer sequential magnetron sputtering," *J. Alloys Compd.*, vol. 800, pp. 272–278, Sep. 2019. doi:10.1016/j.jallcom.2019.06.017

[21] M. S. Shakel *et al.*, "$Nb_3Sn$ coating of a 2.6 GHz SRF cavity by sputter deposition technique", in *Proc. NAPAC'22*, Albuquerque, NM, USA, Aug. 2022, pp. 691-694. doi:10.18429/JACoW-NAPAC2022-WEPA30

[22] M.S. Shakel, H.E. Elsayed-Ali, G. Eremeev, U. Pudasaini, A.M. Valente-Feliciano, "First results from $Nb_3Sn$ coatings of 2.6 GHz Nb SRF cavities using DC cylindrical magnetron sputtering system, 2023, doi:10.48550/arXiv.2307.08806

[23] M. S. Shakel, M. N. Sayeed, G. V. Eremeev, A.-M. Valente-Feliciano, U. Pudasaini, and H. E. Elsayed-Ali, "Commissioning of a two-target DC cylindrical magnetron sputter coater for depositing $Nb_3Sn$ film on Nb superconducting radiofrequency cavities," *Bull. Soc. Vac. Coaters*, vol. 217, p. 112563, Nov. 2023. doi:10.1016/j.vacuum.2023.112563

[24] E. Viklund, D. N. Seidman, S. Posen, B. M. Tennis, and G. Eremeev, "Healing gradient degradation in $Nb_3Sn$ SRF cavities using a recoating method," *APL Mater.*, vol. 12, no. 7, Jul. 2024. doi:10.1063/5.0218739